Environmental Science & Technology

pubs.acs.org/est

Article

Soil Buffering Capacity Can Be Used To Optimize Biostimulation of Psychrotrophic Hydrocarbon Remediation

Steven D. Mamet,* Amy Jimmo, Alexandra Conway, Aram Teymurazyan, Alizera Talebitaher, Zisis Papandreou, Yu-Fen Chang, Whitney Shannon, Derek Peak, and Steven D. Siciliano*

Cite This: *Environ. Sci. Technol.* 2021, 55, 9864−9875

Read Online

ACCESS | Metrics & More | Article Recommendations | Supporting Information

ABSTRACT: Effective bioremediation of hydrocarbons requires innovative approaches to minimize phosphate precipitation in soils of different buffering capacities. Understanding the mechanisms underlying sustained stimulation of bacterial activity remains a key challenge for optimizing bioremediation—particularly in northern regions. Positron emission tomography (PET) can trace microbial activity within the naturally occurring soil structure of intact soils. Here, we use PET to test two hypotheses: (1) optimizing phosphate bioavailability in soil will outperform a generic biostimulatory solution in promoting hydrocarbon remediation and (2) oligotrophic biostimulation will be more effective than eutrophic approaches. In so doing, we highlight the key bacterial taxa that underlie aerobic and anaerobic hydrocarbon degradation in subarctic soils. In particular, we showed that (i) optimized phosphate bioavailability outperformed generic biostimulatory solutions in promoting hydrocarbon degradation, (ii) oligotrophic biostimulation is more effective than eutrophic approaches, and (iii) optimized biostimulatory solutions stimulated specific soil regions and bacterial consortia. The knowledge gleaned from this study will be crucial in developing field-scale biodegradation treatments for sustained stimulation of bacterial activity in northern regions.

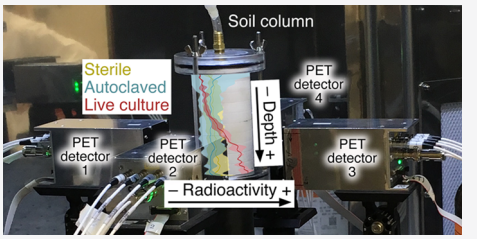

KEYWORDS: *bioremediation, biodegradation, phosphate, positron emission tomography, permafrost, microbial ecology*

INTRODUCTION

Worldwide, polluted sites contribute to ∼2 million deaths each year through soil and water pollution.[1] The carbon cost of cleaning the world's ∼20 million contaminated sites using ex situ methods is 177 billion tonnes of CO_2 equivalents, five times what the entire globe emits each year. Collectively, contaminated sites represent $10 trillion United States dollars (USD) in environmental liability, and costs to the global economy are between $0.2 and $1.1 trillion USD/year (0.25−1.89% of global GDP).[2] Despite the urgent need to reduce the economic and health effects of contaminated sites, current technologies are not up to the task with only ∼5% of sites being remediated.[3] These low rates of remediation activity will, in the worst case, lead to doubling of contaminated sites over the next decade,[2] or, best case, merely equal the rate of new site pollution.[4]

In situ bioremediation is a carbon- and resource-efficient means of depleting hydrocarbons in soil. An in situ biostimulation system for an average site of 3800 m^3 diverts more than 8 kilotonnes of contaminated soil from landfills, avoids the emission of 30 kilotonnes of CO_2 equivalents,[5] and has a cost point typically 30−70% less than excavation-based approaches. The fundamentals of in situ biostimulation have been known for over 50 years[6,7]—providing nutrients and electron acceptors. However, the sustained stimulation of the bacterial activity has proven to be challenging, especially in northern regions[8] where ecosystems may be more sensitive to contamination than southern climes.[9]

Cold, northern regions are characterized by low levels of N and P, which hinder natural source zone depletion (NSZD) of hydrocarbon-contaminated soils.[10] NSZD describes the collective, naturally occurring dissolution, volatilization, and biodegradation processes underlying mass losses of petroleum hydrocarbons (PHCs).[11] Furthermore, biostimulation of bacterial activity in soil decreases over time due to the formation of secondary phosphorus minerals as the biostimulatory solution permeates and reacts with soil matrices. For example, soil mineralogy that favored brushite ($CaHPO_4 \cdot 2H_2O$) formation during biostimulation enhanced hydrocarbon degradation, whereas Ca-deficient soils in which newberyite ($MgHPO_4 \cdot 3H_2O$) formed showed slower hydrocarbon degradation.[12] One solution is the use of ligands[13,14] that chelate Ca and Fe and prevent phosphorus precipitation. Such chelators can help sustain bioremediation.[15] However, biostimulatory solutions also slowly dissolve soil carbonates. Carbonate dissolution releases Ca and Mg, which in turn cause

Received: February 17, 2021
Revised: June 9, 2021
Accepted: June 10, 2021
Published: June 25, 2021

https://doi.org/10.1021/acs.est.1c01113
Environ. Sci. Technol. 2021, 55, 9864−9875

the precipitation of Ca/Mg phosphate minerals, which are less bioaccessible to microbes than adsorbed or dissolved P. If we assume that phosphorus must remain bioavailable for hydrocarbon bioremediation to occur,[15,16] then approaches that modify biostimulatory solutions to minimize phosphate precipitation in soils of differing buffering capacities should outperform standard, one-size-fits-all approaches toward microbial biostimulation.

A wide range of bacteria anaerobically degrade hydrocarbons,[17] and thus, some biostimulatory approaches add nutrients to maintain a C/N ratio of approximately 10 to optimize the metabolic activity.[18] Anaerobic degradation of hydrocarbons by consortia involves not only degraders but also bacteria involved in phosphorus[19] and necromass recycling.[20] Thus, it is reasonable to hypothesize that the addition of oligotrophic biostimulatory solutions might be as effective as traditional, nutrient-rich biostimulatory solutions. If so, then the use of oligotrophic biostimulatory solutions would solve many practical delivery problems associated with distribution system fouling by bacterial overgrowth. Our goal is to test two hypotheses: (1) optimizing phosphate bioavailability in soil would outperform a generic biostimulatory solution in promoting hydrocarbon remediation and (2) oligotrophic biostimulation would be more effective than eutrophic approaches.

Most microcosm designs include variations on a theme in which soil is dried, sieved, and then spiked.[21−23] This process alters the soil surface area coming into contact with the biostimulatory solution, the soil structure, solution flow through fractured clay minerals, the distribution and properties of hydrocarbons, as well as the microbial population and habitat.[24] To better replicate field conditions, intact soil columns can be used.[25] Incremental sampling approaches can help obtain more representative samples for chemical and genomic analysis[26−28] though methods to link activity in soil volumes 10 billion times larger than a genomic sample are needed.

Positron emission tomography (PET) can image over 1.5×10^{-4} m^3 of soil to identify 1.5×10^{-9} m^3 volume of active microbial activity.[29] Thus, PET can provide greater spatial resolution than genomic approaches and is an invaluable tool for characterizing microbial metabolic processes.[30] PET images the gamma rays released from radiotracers such as fluorine-18 (^{18}F), carbon-11 (^{11}C), or nitrogen-13 (^{13}N) that emit positrons which travel a short distance, ∼1 mm in water, before releasing gamma radiation due to antimatter/matter interactions (annihilation).[30] Using fluorine-18 ($[^{18}F]F^-$) to track water flow through a core followed by a glucose analogue 2-[^{18}F]fluoro-2-deoxy-D-glucose ([^{18}F]F-FDG), one can map the heterotrophic microbial metabolism of exogenous *Rahnella*[31] and indigenous sediment bacterial communities.[32] Here, we used a similar approach to quantify and visualize bacterial activity in intact soil cores obtained from a subarctic contaminated site in which in situ biostimulation was being considered. In so doing, we could not only test our project hypotheses but also evaluate if the optimized biostimulatory solutions (i) increased generalized biomass or (ii) selectively stimulated only certain regions and types of bacteria.

MATERIALS AND METHODS

Site Description and Field Data Collection. The field site was in Old Crow, YT, situated immediately downstream of the confluence of the Porcupine and Old Crow Rivers, approximately 130 km north of the Arctic Circle. The site is complex in its geological and hydrogeological profiles, further complicated by the underlying continuous permafrost, cryosolic soils experiencing cryoturbation, and a seasonally fluctuating active layer. The soils are mainly wet, medium-plastic olive-gray silts, with trace organics. As of 2017, diesel contaminants were present in the soil at the field site at concentrations exceeding the Yukon Contaminated Sites Regulations Residential Land Use standards and Special Waste Regulations standards. In September 2017, intact soil cores (n = 19) were collected at a depth of 0.25−0.50 m below the ground surface from nine locations representing ∼250 m^2 across the site in 90 mm outer diameter steel Shelby tubes either 760 or 460 mm in length.[33]

Biostimulatory Rationale. The Base biostimulatory solution consisted of 800 mg L^{-1} HNO_3, 180 mg L^{-1} tripolyphosphate (TPP), 100 mg L^{-1} $MgSO_4$, and 6.29×10^4 mg L^{-1} Fe(III)NH_4-citrate to have a C/N/P ratio of 100:11:1 based on the hydrocarbons present in the soil (see Table S1 and Supporting Methods). The oligotrophic version of this solution had much lower N and P concentrations, 3.4 mg L^{-1} HNO_3 and 3.1 mg L^{-1} TPP. To create the Focus biostimulatory solutions, we developed a decision tree to customize the biostimulatory solution for each core (Figure S1). We first assessed if the soil buffering capacity was high (pH > 4.5 after addition of 10 mM citrate buffer) and then if the soil was Ca-rich (Mg:Ca < 0.12) and finally Fe-rich ($Fe_{solution}$ > 30 mg L^{-1}).

Field soil cores and biostimulatory experiment. We created microcosms (n = 4−7 per core, depending on the core length, 131 in total), an intact soil core inside a polyvinyl chloride tube measuring 3.5 cm in diameter and 5 cm in height, from each soil core. Each microcosm was placed into a 125 mL amber jar with a treatment solution for 28 days at 4 °C to mimic in situ temperatures and allowed to go anaerobic. Microcosms were placed on a rotary shaker set at 2.5 s^{-1}. The rotary shaker was used to reproduce groundwater flow conditions as much as possible with the microcosm setup and to maximize surface interactions. Shaking was carried out at a relatively low speed to reduce potential siltation and matrix interferences during the analytical tests.

Treatment solutions (Table S1 and see below) were one of: Control (distilled and deionized (DI) water; n = 37), Base (solution of nitrogen, phosphate, ammonium iron(III) citrate, and sulfate; n = 45), Focus (slight modifications of the base solution based on the decision tree; n = 26), and Focus + Oligo (same modifications as corresponding to Focus treatment however with lower N and P concentrations (i.e., slightly oligotrophic); n = 23). On the second day of the experiment, we sampled and replenished 50 mL of each microcosm solution and analyzed for nutrient concentrations (see Figure S2). After 28 days, 12 microcosms were selected and kept intact for PET analysis (eight base solutions and four DI water solutions). The selection criteria were as follows: from the cores that showed successful degradation with the Base solution, we narrowed down our microcosm options by removing any microcosms that had noticeable slumping as cores shorter than 4 cm could not be imaged well. Microcosms were then randomly selected from the remaining number left. For the remaining unselected microcosms, soil was extruded, homogenized by hand mixing, and subsampled for DNA, exchangeable nutrients, and PHCs.[12]

https://doi.org/10.1021/acs.est.1c01113
Environ. Sci. Technol. 2021, 55, 9864−9875

The biostimulatory experiment combined two experiments: the first one evaluated DI water and Base (n = 4 soil cores; microcosms—DI: n = 22 and Base: n = 24) and the second one included Focus and Focus + Oligo (n = 15 cores; microcosms—DI: n = 15, Base: n = 21, Focus: n = 26, and Focus + Oligo: n = 23). The first experiment had an even number of DI and Base microcosms created from two cores, while the other two cores had an uneven number, and we used the Base treatment for these two. As mentioned previously, we had enough soil for a varying number of microcosms from each core (4−7). Each core had a minimum of n = 1 mesocosm for each treatment (DI, Base, Focus, and Focus + Oligo). For cores from which we were able to extract more microcosms, we prioritized Focus and Focus + Oligo treatments because we had completed more DI and Base microcosms from the first experiment. The first pilot experiment indicated the variability within the success of the Base solution, which prompted us to conduct the second experiment considering the Focus and Focus + Oligo treatments. Both experiments followed the same protocol detailed here and thus our analyses focus on the results from both.

Verification of PET and the dosing system. We used model cores to verify that our imaging system and microcosms could differentiate between $[^{18}F]F^-$ water paths and [^{18}F]F-FDG retention by bacteria. Three model cores (see below) were pushed into a Tempe cell (Soil Moisture Equipment Corp., Santa Barbara, CA) modified with a Teflon barrel. Each Tempe cell has an inflow and an outflow with 1 bar ceramic plate filters sealed with an O-ring that is used to determine the movement rates through the soil and the physical and chemical soil properties.

The model cores had three layers (15 mm in height) of sterilized silica sand (DS2000/SIL4, SIL Industrial Minerals, Bruderheim, SK) inside the Tempe cells (Figure S3). Each layer was 15 mm thick and 35 mm in diameter with a total height of 45 mm. All cores had dry sand as the top and bottom layers; however, the middle layers were either: (a) infused with 2 mL of Milli-Q water, (b) inoculated with *Pseudomonas* (isolated from environmental soil samples, identified using API strips, bioMérieux, St. Laurent, QC) in 2 mL of Milli-Q water and then autoclaved at 121 °C under 110 kPa, or (c) inoculated with *Pseudomonas* in 2 mL of Milli-Q water.

We injected the model cores with ∼16 MBq [^{18}F]F-FDG in 42 mL of DI water, waited for ∼10 min, and imaged in the scanner mode. Thereafter, three pore volumes (∼63 mL) of DI water was pushed through the cell at 1 bar pressure to wash out residual [^{18}F]F-FDG and imaging was conducted again in the scanner mode. For the soil cores, we injected 42 mL of ∼13 MBq [^{18}F]F-FDG solution into the core, which was then washed with 145 mL of DI water. We then autoclaved the core and then treated again with 42 mL of ∼16 MBq [^{18}F]F-FDG solution and washed with 155 mL of DI water. For all cores, we measured the outflow to determine the volume taken up in the core.

Modular PET System. The custom-built PhytoPET system used here consisted of four 60 mm × 60 mm × 124 mm detector modules.[29] Detailed information and characterization of the electronics and the data acquisition architecture can be found in previous studies.[34−36] A 360 degree rotation stage and a 50 cm translation stage were incorporated to allow relative movement between detectors and objects for continuous step-and-shoot acquisition.[37]

To calibrate volume estimates from the PET imagery, we used radioactive volume dimensions in PET images of the NEMA NU 4-2008 image quality phantom.[38] During calibration, a threshold factor applied to the image stack was chosen to best separate radioactive volumes from the background based on their intensity and to allow the feature dimensions in the PET images to reflect the real phantom feature dimensions. The signal count rates of the phantom used for this calibration process were at the same order as those used in the experiments herein. The phantom comprises radioactive volume features with dimensions ranging from 1 to 30 mm. To avoid overestimating the volumes based on the PET images, the phantom feature dimensions equal to or larger than 3 mm were taken into account in the calibration process. This corresponded to an activity threshold of 0.504× maximum activity within each image stack to separate radioactive voxels from the background for volume estimates.

Camera mode images were reconstructed with proprietary software[35] employing the iterative maximum likelihood expectation maximization algorithm[39] based on a voxel size of 0.5 mm^3 and 50 iterations. For the scanner mode, data were preprocessed using in-house developed code and together with the corresponding crystal positions and directions were fed into a modular tomographic image reconstruction platform (CASToR) for list-mode image reconstruction.[29,40] Raw images were exported and processed using the Fiji distribution[41] of ImageJ.[42] To calculate activity volumes for each core, we used an activity threshold of 0.504× maximum activity (see above) within each image stack. We trimmed the data outside the diameter of the core (>35 mm) and excluded data outside 4.6−42.5 mm range to avoid field-of-view and pooling effects. We calculated volumes using the Just Another Colocalization Plugin (JACoP) in Fiji.[43]

Bacterial versus Soil Pore Volumes. Bacteria are metabolically agnostic to $[^{18}F]F^-_{(aq)}$, which makes it an ideal radiotracer to quantify open soil voids unoccupied by bacteria. Conversely, as an analogue of glucose, [^{18}F]F-FDG shows high uptake by bacteria.[44] Therefore, we used PET imaging of [^{18}F]F-FDG to obtain estimates of open pore plus bacterial volumes and subtracted the pore volumes determined through imaging of $[^{18}F]F^-_{(aq)}$ to quantify bacterial volumes in four soil cores (two DI water and two base biostimulatory solution treatments).

Imaging Pore Volumes and Bacterial Activity in Intact Cores. The field soils had a mean bulk density of 1.47 g cm^{-3} and a mean void volume of 26.37 cm^3. Thus, approximately 27 mL of solution would completely fill the void volumes of an intact 5 cm × 3.5 cm core. The soil pH was ∼6.8, and there were approximately 700 mg L^{-1} $CaCO_3$ and 0.5 mg L^{-1} phosphate in the system. Thus, before adding fluorine-18, we exchanged the high pH solution with DI water to prevent fluoride coprecipitation with Ca or P. For each field soil core, we washed out Ca/P with 81 mL (three void volumes) of DI water under 1 bar of pressure.

We injected 54 mL of 4.2 MBq $[^{18}F]F^-_{(aq)}$ (0.1 MBq mL^{-1}) solution to the top of the Tempe cell under 1 bar of pressure until 18 mL exited the cell. Each core was then imaged using the PhytoPET system for 5 min. Immediately after imaging, we pushed 3× pore volume (81 mL) of DI water through the Tempe cell to wash out the remaining $[^{18}F]F^-_{(aq)}$. Next, we added 54 mL of 42 MBq [^{18}F]F-FDG (1 MBq mL^{-1}) to the top of the Tempe cell until 27 mL exited the core. The core was incubated for 90 min following [^{18}F]F-FDG application

https://doi.org/10.1021/acs.est.1c01113
Environ. Sci. Technol. 2021, 55, 9864−9875

and then 27 mL of DI water was pushed through at 1 bar to remove residual [^{18}F]F-FDG leaving only [^{18}F]F-FDG inside bacterial cells. After washing, the core was imaged for 5 min.

After imaging and all solutions were flushed through, we extruded the cores by pushing out 1 cm of soil at a time to maintain the orientation of the core. Each 1 cm soil puck (n = 5 per cylinder) was subsampled nine times (once in each 45° quadrat and once in the middle) using glass pipettes. Gamma radiation in each subsample was measured using a 2480 Wizard2 1-detector gamma counter (PerkinElmer, USA). Subsamples were maintained at −80 °C for DNA analyses. PHC fractions were grouped according to the equivalent normal straight-chain hydrocarbon (nC) boiling point ranges and were defined by four fractions (F1−F4).[45] The remaining soil in each puck was homogenized and analyzed for F2 (>nC10 to nC16) and F3 (>nC16 to nC34) concentrations and moisture.

16S rRNA Sequencing. We subsampled the soil pucks for bacterial composition determination, taking between 9 and 19 soil samples per core (n = 150 subsamples). Some soil locations could not be subsampled due to rocks, voids, etc. We used quantitative polymerase chain reaction (qPCR) to quantify rRNA from each subsample. RNA was extracted using an RNA mini kit (Zymo Research), and concentrations were determined using an Invitrogen Qubit RNA HS Assay Kit (Thermo Fisher Scientific). We used reverse-transcription PCR (RT-PCR) and oligo(dT) for cDNA synthesis (Invitrogen, Thermo Fisher Scientific). For amplification of the 16S rRNA gene, we used a reaction mixture containing 18.2 μL of H_2O, 2.5 μL of DreamTaq buffer (Invitrogen by Thermo Fisher Scientific), 1 μL of each primer (342F (5′-CTA CGG GGG GCA GCA G-3′) and 806R (5′- GGA CTA CCG GGG TAT CT-3′)), 0.05 μL of each nucleotide (dATP, dCTP, dGTP, and DTTP), and 0.125 μL of Taq polymerase with a 35 cycle PCR. Each sample was spiked with a known concentration of *Aliivibrio fischeri* (*A. fischeri*) as an internal standard.[46] Samples were purified using NucleoMag Magnetic Beads (D-Mark Biosciences), indexed for 16S rRNA sequencing (Illumina), and purified again. After pooling, samples were sequenced on an Illumina MiSeq using a V3 Chemistry kit (600 cycle).

qPCR. We used qPCR with primers targeting a fragment of the 16S rRNA gene to quantify DNA expression in soil subsamples of different radioactivities. qPCR was run using an Applied Biosystems 7500 Real Time PCR System (Thermo Fisher Scientific, Toronto, ON), and SYBR green was used to quantify the bacterial DNA obtained with the 342F/806R primers to target our regions of interest in the 16S rRNA gene. We used the 16S rRNA gene due to its valuable uncommon properties (ubiquity, extreme sequence conservation, and a domain structure with variable evolutionary rates), which makes it easy to distinguish between different genera and it is the *de facto* standard for prokaryotic taxonomy.[47,48] Each 20 μL reaction mixture contained the following: 10 μL of SYBR Green master mix (QIAGEN Instruments, Toronto, ON), 1 μL of 10 μM of each forward and reverse primers, 2 μL of 5 ng/μL DNA,[49] and 6 μL of nuclease-free H_2O. The normal standard ranged from 10^5 to 10^8 copies/μL. The coefficients of determination (R^2) for our assays ranged from 0.95 to 0.99, while amplification efficiencies were between 0.85 and 0.99. Based on the melting curve analyses, we found no evidence for primer dimers. The resulting quantities of rRNA gene copies were normalized by expressing gene copies as ratios to the maximum quantity of copies per replicate.

Bioinformatics. A total of 6,677,295 reads were produced with an average of 44,515 reads per sample. Primers were removed using cutadapt v.2.1[50] and then imported into QIIME2 v.2020.8.[51] Sequences were joined using VSEARCH[52] and then filtered based on quality using default parameters: maximum number of consecutive low-quality scores (r = 3), minimum length that a sequence read can be truncated and still be retained (p = 0.75 total read length), maximum number of low PHRED scores that can be observed in direct succession before truncating a sequence read (q = 3), maximum number of ambiguous (i.e., N) base calls (n = 0), minimum four sequence count (c = 0.005%),[53] and sorting into amplicon sequence variants (ASVs) using a trim length of 400 in Deblur.[54] ASVs were classified using a 342F/806R-trained V3/V4 SILVA database.[55] The resultant QIIME2 abundance and taxonomy artifacts were exported to BIOM format[56] for processing in R v.4.0.2[57] and combined with sample information using "phyloseq" v.1.26.1.[58] Chloroplasts and mitochondrial contaminants were removed, and abundances were standardized to the *A. fischeri* spike.[46] Finally, we removed any ASVs with a mean read count ≤1 and/or samples with ≤1 nonzero value. There were 720 unique ASVs with an average of 70 ASVs and 41,414 reads per sample across 141 samples in the final data set. Each ASV was present in 2−128 samples with a mean prevalence of 13. A phylogenetic tree was constructed by inserting the sequences in the Greengenes 13_8 reference tree[59] with the QIIME2 plugin "q2-fragment-insertion"[60] using the SATé-enabled phylogenetic placement method.[61] The tree was exported from QIIME2 in Newick format,[62] imported into R using the "ape" package v.5.4,[63] and plotted using "phylosignal" v. 1.3[64] and "phylobase" v. 0.8.10.[65]

Statistical Analyses. *PHC Degradation.* PHC degradation rate constants (k) were determined using single first-order kinetics

$$k = -\left(\frac{\ln(C_t) - \ln(C_0)}{t}\right)$$

where C_t is the concentration at time t and C_0 is the starting concentration. Preliminary linear models indicated that the core depth below the surface and initial PHC concentrations influenced the degradation constants. To maximize our inferential power about biostimulatory treatment effects, we fit a series of generalized least-squares (GLS) linear models testing the influence of depth, initial concentrations, and their interaction with degradation constants using the "nlme" package v.3.1−148 in R.[66] We used model selection to determine the variance structure for heterogeneity in model residuals and the most predictive combination of fixed effects.[67] We modeled variance heterogeneity using an exponential variance structure in these initial models. Once we generated the model of best fit (assessed using Akaike Information Criterion), we calculated residuals from those best fit models to use as bias-free estimates of degradation constants in downstream assessments of treatment effects (Table S2). For the downstream analyses of treatment effects, we used a different variance spread per treatment ("varIdent") to address variance heterogeneity and maximize the model fit (Table S2).

P Immobilization. P immobilization was calculated as the difference between initial and final phosphorus in solution. To account for different initial phosphorus concentrations among

https://doi.org/10.1021/acs.est.1c01113
Environ. Sci. Technol. 2021, 55, 9864−9875

cores, we normalized immobilization by input concentrations. Similar to that mentioned above, we fit a series of GLS models to test the influence of depth on P immobilization rates (Table S2). No depth relationship or variance heterogeneity was detected, so linear models were used to assess treatment effects.

Bacterial Composition. We assessed the microbial community composition using principal component analysis (PCA), and compositional differences were quantified using both redundancy analysis (RDA) and permutational multivariate analysis of variance in the "vegan" v. 2.5−7 package in R.[68] To address the compositional nature of the bacterial microbiome, zeros in the data set were replaced using a geometric Bayesian multiplicative approach using the "zCompositions" v.1.2.0 R package and then transformed using a centered-log ratio (CLR) transformation using the "CoDaSeq" v. 0.99.3 package.[69−71] The CLR mitigates the issue of differences among microbial taxa not being linear by turning the read counts into a ratio abundance (abundance normalized by the geometric mean abundance of all taxa per sample). CLR allows us to retain the relationships among samples and also puts the data in a linear space where we can apply linear statistical techniques such as PCA. The geometric mean centers the abundance values such that the average relative abundance is zero and therefore above average abundances will be positive and below average will be negative. We used RDA to assess the bacterial compositional differences among treatments.

RESULTS

Optimizing PHC Degradation by Optimizing P Accessibility. The Focus treatment tripled F3 degradation rate constants compared to the Base treatment (0.006 ± 0.004 and 0.021 ± 0.009 day^{-1} in the Base and Focus, respectively) (Figure 1 and Table S2; constants are means ± SE). Only Focus and Focus + Oligo (0.016 ± 0.006) rate constants were significantly ($P < 0.05$) greater than DI water rates (0.003 ± 0.004 day^{-1}). These increased degradation rates correspond to half-life times of 231 days for DI water, 115 days for Base, and 33 days for Focus. The effect of initial F3 concentrations on degradation rate constants was minimal and soil depth had no influence (Table S2).

The increased degradation of hydrocarbon fraction F3 was not necessarily linked to increased P availability for microorganisms (Figure 2a,b,f) as P immobilization/fixation was greatest in our Focus + Oligo treatment (0.492 ± 0.190; though immobilization was still relatively high in the focus treatment: 0.203 ± 0.111 versus 0.058 ± 0.027 in the DI control). Though increased NH_4^+ versus NO_3^- availability likely played a role in increased F3 degradation (Figure 2c−e,g), we were unable to verify P mineralization on samples due to an experimental error during transfer to the Canadian Light Source that damaged the PET-imaged samples.

The Focus treatment (0.013 ± 0.009) did not improve the Base F2 degradation rates of 0.024 ± 0.012 day^{-1}, which were greater ($P < 0.056$) than the DI water rates (0.001 ± 0.01 day^{-1}). Like F3, the initial concentrations of F2 had little influence on degradation activity but soil depth did, with F2 degradation rates decreasing as the soil depth increased.

Bacterial and Soil Pore Space Volumes. Soil porosity estimates using radiotracers corresponded with estimates based on bulk density (Table 1). Bacteria occupied between 60.3 and 74.4% of the total pore space, representing between 29.8 and 40.8% of the total soil volume (Table 1 and Figure 3a). The bacterial volume was 17.6 cm^3 in the Base treatment compared to 15.6 cm^3 in the DI treatment but these volumes were not statistically different ($P > 0.05$). We were unable to assess the Focus treatment as we were only able to assess four cores using radiotracers.

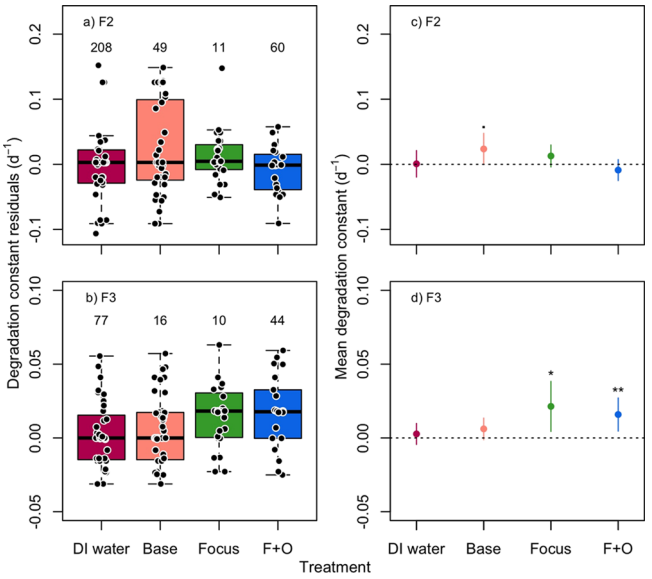

Figure 1. Treatment influence on PHC degradation. F + O indicates focus plus oligo. Degradation constant estimates for hydrocarbon fractions (a) F2 and (b) F3. Degradation constants represent the residuals from GLS modeling degradation based on depth within the soil core and initial PHC concentrations. C/N ratios are presented above each treatment. Mean degradation constants (c,d) from GLS models estimating treatment influence. ·,*, and ** denote significance at $P < 0.1$, 0.05, and 0.01, respectively. Error bars represent 95% confidence intervals. Note the scale difference between *y*-axes for F2 and F3. See the Supporting Information (Table S2) for more details about the models.

There are largely three types of pores present in these soils (Figure 3b): (i) bacterial microcolony pores where the pore space is filled with active bacteria but through which water can flow, (ii) biofilm pores in which there are channels of pores free of active metabolic activity through which water flows, and (iii) inaccessible pores where no bacteria or water flows (Figure 3b, black pixels; also see Figures S4 and S5).

Biostimulation of Bacterial Activity as Measured by [^{18}F]F-FDG Incorporation. We successfully labeled *Pseudomonas* in sand cores with [^{18}F]F-FDG (Figures S6 and S7). Radioactivity was greater in live *Pseudomonas* cores relative to sterile and autoclaved samples, with some downward movement of the bacterium with [^{18}F]F-FDG and DI water flow. Radioactivity in field soil cores treated with the base biostimulatory solution was associated with 16S rRNA gene expression ($t_{55} = 8.705$, $P < 0.001$) and no relationship was detected in the DI water treatment (Table 2 and Figure 4). Incorporated radioactivity in Base-stimulated soils (mean ionization event counts per minute per gram of soil ± SE = 180,896 ± 51,084) was 108% that of DI water-treated soils (86,981 ± 19,893), and similarly 16S rRNA expression was 10-fold greater in Base-stimulated soils. If we only compare samples between DI and Base with similar levels of radioactivity, the link between incorporated radioactivity and 16S rRNA expression remains. As a quality control check, in field soil cores with indigenous microbes, radioactivity was

https://doi.org/10.1021/acs.est.1c01113
Environ. Sci. Technol. 2021, 55, 9864−9875

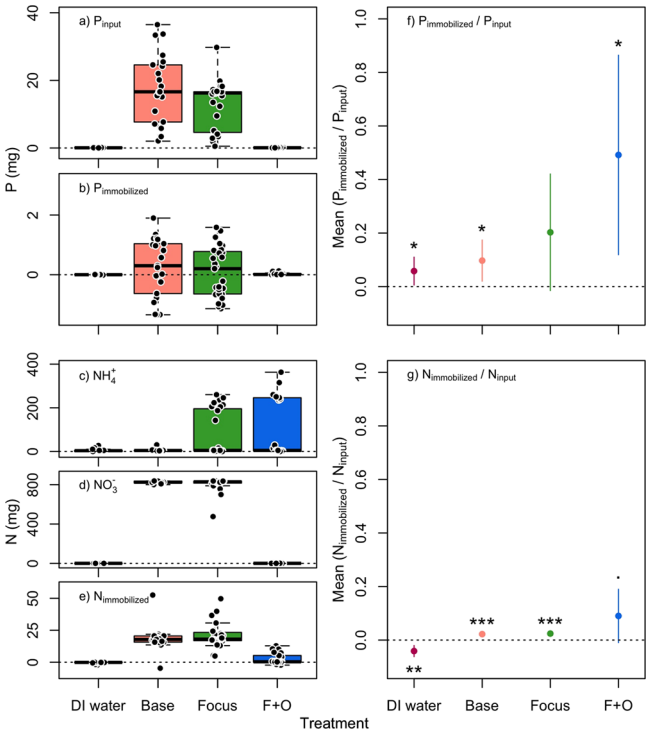

Figure 2. Phosphorus and nitrogen cycling and the influence of treatment on each. F + O indicates focus plus oligo. (a) Input P and (b) immobilized P for each treatment. Organic input N consisting of (c) ammonium (NH_4^+) and (d) nitrate (NO_3^-). Thus, $N_{input} = NH_4^+ + NO_3^-$. (e) Immobilized N for each treatment. Mean (f) P- and (g) N-immobilization normalized by input concentrations from GLS models estimating the treatment influence. ·,*,**, and *** denote significance at $P < 0.1$, 0.05, 0.01, and 0.001, respectively. Error bars represent 95% confidence intervals.

greater throughout the soil profile relative to the autoclaved field soil cores (Figure S8).

Bacterial Community Composition. There were 1030 ASVs across 141 samples from the QIIME2 pipeline. After *A. fischeri* standardization and removal of singletons/doubletons, 720 ASVs were remaining. Of these 720, 96 were unique to the Base treatment consisting of seven phyla (Figure 5a,b) and an additional 87 were more than double[72] the relative abundance in the DI treatment (Table S3). The 96 unique taxa in the Base treatment consisted of 59 genera from Proteobacteria, 16 Firmicutes, 11 Actinobacteria, 6 Bacteroidetes, 2 Chloroflexi, 1 Hydrogenedentes, and 1 Gemmatimonadetes.

Not surprisingly, the most abundant genus in the Base treatment was *Pseudomonas*, a known hydrocarbon degrader (Figure 5a and Table S3). There were other known degraders from Gammaproteobacteria (*Stenotrophomonas*: $n = 4$) and Alphaproteobacteria (*Sphingomonas*: $n = 3$) that were either absent in the DI water treatment or much more abundant in the Base treatment. Several other genera relevant to bioremediation were abundant in both base and DI treatments. For instance, known carbon cyclers like *Cellulomonas*, *Geobacter*, and *Rhodoferax*[73−75] had relative abundances >1% in both treatments (Figure 5c). Other carbon cyclers from the OPB41 and Solirubrobacterales orders[74,76] were noticeably differentially abundant between the base and DI treatments (178- and 357-fold greater in base; Table S3). Known syntrophs like *Syntrophus*, *Smithella*, and *Thauera*[75,77] were also present, albeit in lower (<1%) relative abundances. Interestingly, the largest fold-change detected between base and DI treatments was for a known phosphate-solubilizing Alphaproteobacteria *Methylobacterium*, which was >740-fold more abundant in the Base treatment (Figure 5a and Table S3). Another phosphate-solubilizing genus from Actinobacteria, *Corynebacterium*,[78] was 42-fold more abundant in the Base versus DI water treatments.

[^{18}F]F-FDG incorporation did not predict community composition changes (Figure S9) despite differences in community composition between Base and DI treatments (RDA: $F_{1,139} = 4.174$, $P = 0.001$). The change in community composition was driven by the 238 ASVs that were at least double the abundance in the Base community. However, two genera of the phylum Proteobacteria, *Polaromonas* (Base: 40% and DI water: 41%) and *Pseudomonas* (Base: 28% and DI water: 16%), comprised over half the community (Figure 5c). Some members of these taxa increased by 1.2−6.3 fold (*Polaromonas*) and 1.1−136.7 fold (*Pseudomonas*) in the Base compared to the DI treatment. Thus, the observed link between [^{18}F]F-FDG and 16S RNA expression (Figure 4) may arise from these two bacteria's ready incorporation of glucose.

DISCUSSION

Using intact soil cores from a diesel-contaminated site in northern Yukon, Canada, we tested biostimulatory solutions that minimize phosphate precipitation in soils of different buffering capacities. Using a combination of microcosm, PET, and genomic approaches, we found that optimized biostimulatory solutions tripled F3 degradation rate constants relative to generic solutions (Figure 1b,d and Table S2) and the rate constants were ∼7× greater relative to that of control (DI water) treatments. A previous study found similar rate differentials in field experiments well south of the Arctic circle.[79] Thus, Focus biostimulatory solutions can provide substantial stimulation of northern hydrocarbon degradation despite unfavorable (e.g., lower temperatures) conditions.

At this field site, using air temperature as a rough proxy for soil temperatures, there are ∼160 days where minimum temperatures are greater than −5 °C[80] and hydrocarbon degradation can occur though the number of days with temperatures greater than −5 °C below the ground surface are likely less than 160. The Canadian Council of Ministers of the

Table 1. Void Characteristics of Microcosms Used in the Volume Experiment

		lab					radiochemistry		
sample	treatment	dry density (g cm^{-3})	bulk density (g cm^{-3})	soil volume (cm^3)	solid volume (cm^3)	porosity (cm^3)	bacterial volume (cm^3)	open pore volume (cm^3)	porosity (cm^3)
1B	DI water	1.23	1.53	47.12	21.83	25.29	14.06	7.18	21.24
4D		1.08	1.35	48.08	19.62	28.46	17.04	9.14	26.18
2A	base	1.28	1.60	46.16	22.24	23.92	18.84	6.49	25.33
4A		1.12	1.40	48.08	20.28	27.80	16.39	10.80	27.19

https://doi.org/10.1021/acs.est.1c01113
Environ. Sci. Technol. 2021, 55, 9864−9875

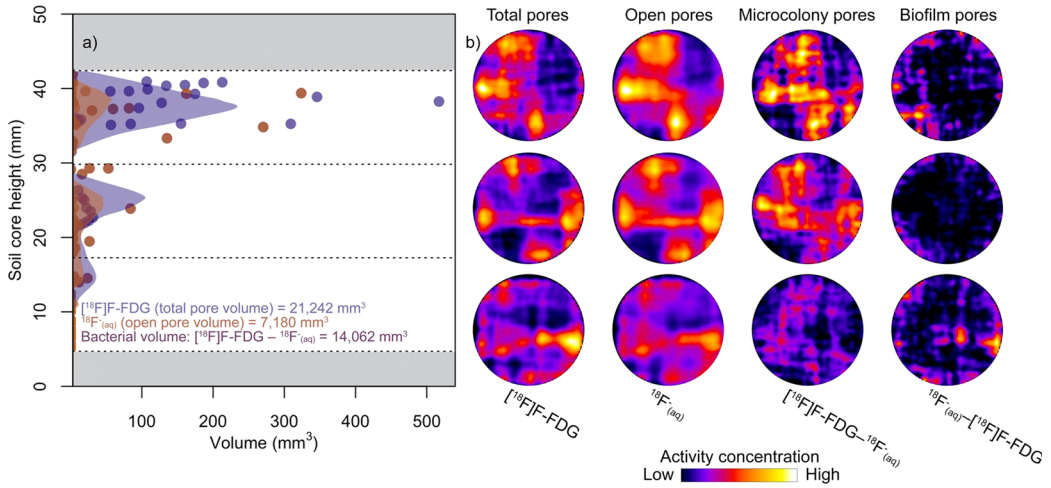

Figure 3. (a) Volume of soil pore space and bacteria in a field soil core, first injected with $[^{18}F]F^-_{(aq)}$ to map the open pore space, rinsed with DI water, followed by injection with $[^{18}F]$F-FDG to map the total pore space, and again rinsed with DI water. Points represent the volume estimates, and the shaded regions are bounded by a Gaussian loess smoother (span = 0.176). The upper polygon (violet) indicates bacterial volume (14,062 mm^3). The lower polygon (dark orange) indicates open pore (7180 mm^3). The sum of the two is the estimate of the total available pore space (21,242 mm^3). Gray rectangles indicate regions that were either out of the field of view of the PET detector (<4.6 mm) or account for label pooling (length >42.5 mm). Horizontal dotted lines indicate the averaged cross sections presented in (b). (b) Mean radioactivity in core cross sections bounded by the dashed lines in (a). Activity concentrations have been standardized relative to the maximum values to facilitate visual comparisons between the $[^{18}F]F^-_{(aq)}$/$[^{18}F]$F-FDG and $[^{18}F]$F-FDG − $[^{18}F]F^-_{(aq)}$/$[^{18}F]F^-_{(aq)}$ − $[^{18}F]$F-FDG images. Actual concentrations were lower in the residual images.

Table 2. Results of Linear Models Examining the Relationship between Radioactivity Retention and 16S rRNA Gene Expression in PHC-Contaminated Soils[a]

covariance parameter estimates	biostimulatory solution	DI water				
random effect on intercept						
soil core ID	0.272	–				
fixed effect estimates	variable	coefficient	SE	d.f.	*t*-value	*P*-value
biostimulatory solution	radioactivity	0.894	0.103	55	8.705	0.000***
	intercept	0.785	0.214	55	3.668	0.001***
DI water	radioactivity	−0.136	0.220	39	−0.620	0.539
	intercept	1.714	0.245	39	6.993	0.000***

[a]***Indicates significance at $P \leq 0.001$.

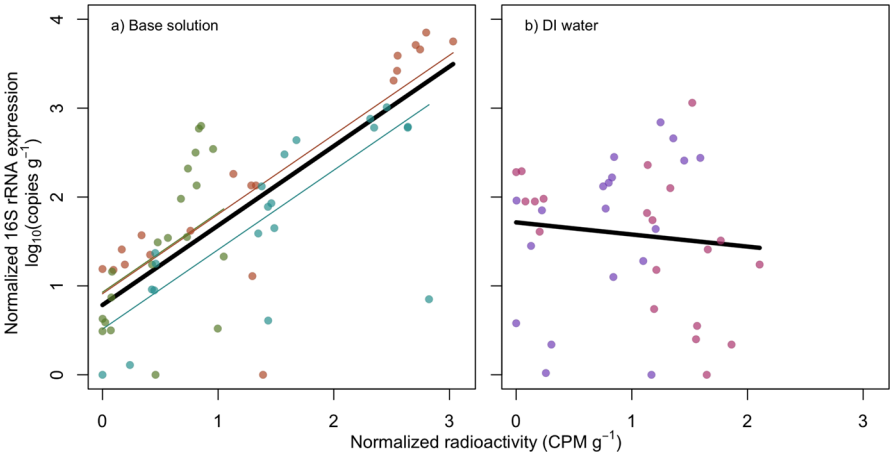

Figure 4. Relationship between soil radioactivity and bacterial 16S rRNA gene expression in PHC-contaminated soil cores following $[^{18}F]$F-FDG permeation and DI water wash. Soil cores were treated with (a) base biostimulatory solution or (b) DI water. Different colors of points indicate unique soil cores. A linear mixed effect random intercept model was fit in (a) and linear regression model in (b) (Table 2). The thick black line indicates the population model and thin lines of varying color in (a) show fits for individual soil cores. (a) $R^2_m = 0.574$ and $R^2_c = 0.636$. (b) $R^2_{adj} = -0.016$.

https://doi.org/10.1021/acs.est.1c01113
Environ. Sci. Technol. 2021, 55, 9864−9875

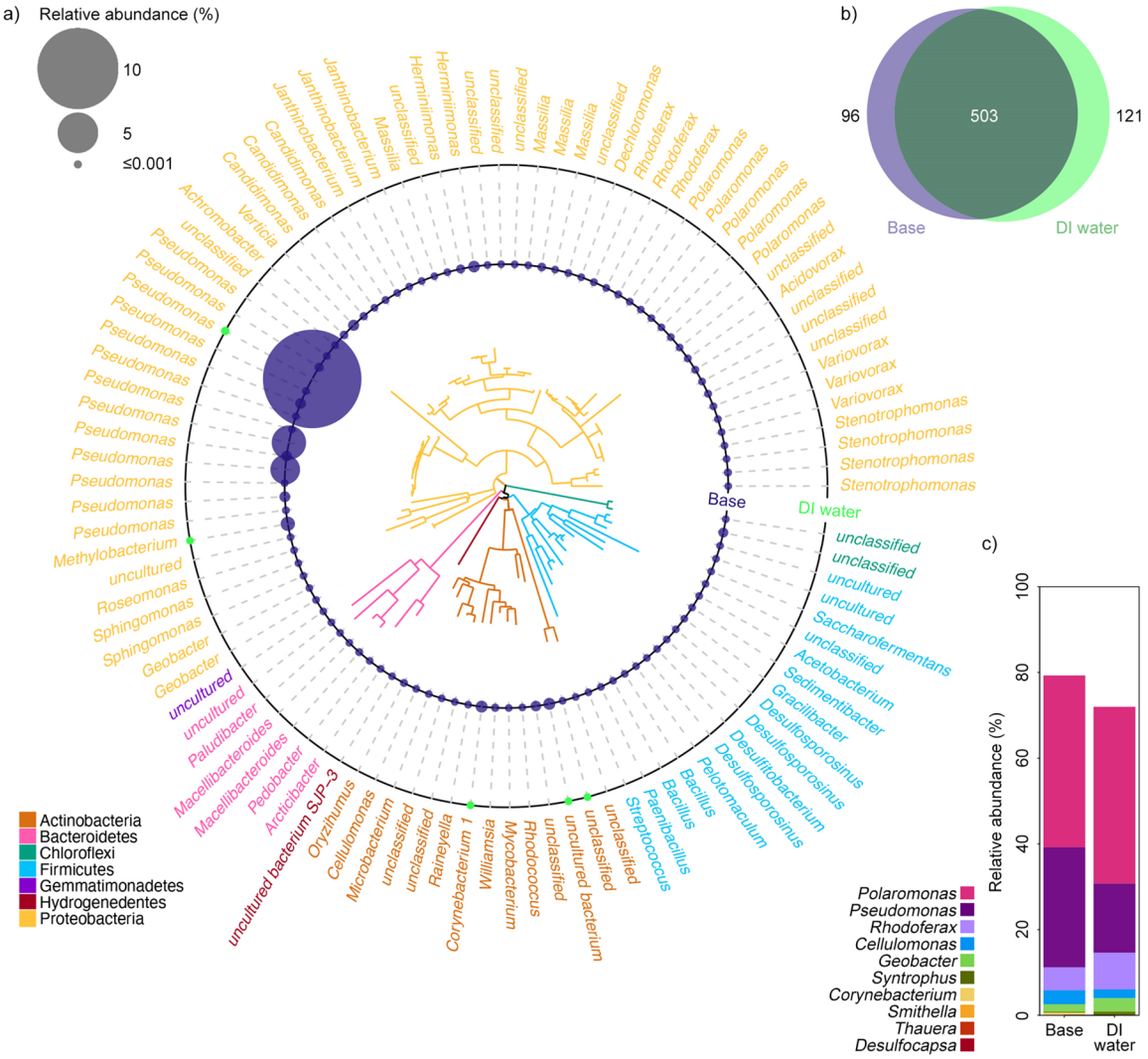

Figure 5. (a) Rooted radial phylogeny of the ASVs with the greatest increases in relative abundance (fold changes >42; $n = 5$) in the Base treatment relative to DI water and ASVs that were present in the Base treatment and absent in DI water ($n = 96$). (b) Venn diagram illustrating the number of shared and unique taxa in treatment. (c) Relative abundance of taxa summed by genus. These 10 taxa represent the top three most abundant genera in both treatments as well as several ecologically relevant bacteria in the context of bioremediation.

Environment (CCME) Tier 1 guidance values for F3 concentrations in coarse-grained soils are 1700 mg kg^{-1}.[45] Using CCME guidelines as a target, the number of days with temperatures greater than −5 °C each year, and the decay constants calculated above, application of the Focus biostimulatory solution could be predicted to close the site within 1 year, compared to 3 years for the Base, or 6 years for NSZD to occur. A similar comparison with half-lives for F2 suggests that the Base solution would result in site closure in approximately 2 years compared to 35 years by NSZD. These results are encouraging though given we are extrapolating from a relatively small number of lab microcosms, we caution readers to interpret these closure times accordingly.

Furthermore, P immobilization in Focus solutions was tripled relative to the control and doubled relative to generic solutions (Figure 2a,b,f and Table S2). Based on these results, we propose that nuanced biostimulatory solutions that optimize soil buffering capacity to improve phosphate bioavailability may provide a means to remediating soils in northern environments though further work on P mineralization is necessary to confirm this result.

Bacteria occupied over half of the pore space in the intact soil cores. There appeared to be three broad types of pore space that could be imaged using ^{18}F-radiotracers. This allows us to explore disparate specialized niches and communal behavior of bacteria and the pore-scale hydrodynamics that influence their habitat. The patchy distribution of microcolonial bacteria that appeared to be most metabolically active is suggestive of heterogeneous resource allocation.[81,82] This may reflect the heterogeneous distribution of diesel and/or nutrients within the soil, which is common in PHC-contaminated soils.[83] Biofilm bacteria typically form through production of extracellular polymeric substances and can dramatically alter the fluid dynamics of their environment.[84] Live and/or dead bacteria may clog preferential flow paths, effectively remodeling the porous network within the soil, with implications for chemical transport in natural porous media. Quantifying the nature of soil pore space is crucial for understanding bioremediation nuances as these spaces determine the hydraulic mechanisms and hot spots of

https://doi.org/10.1021/acs.est.1c01113
Environ. Sci. Technol. 2021, 55, 9864−9875

metabolic activity—key determinants of bioremediation success.

Radioactivity was indicative of gene expression, which was greater in biostimulated soils relative to control treatments (Figure 4 and Table 2). Model sand cores indicated that the increased radioactivity was indeed due to metabolism by live bacteria and not due to bacterial morphology or soil structure (Figure S7). We identified several taxa potentially involved in either anaerobic or aerobic cycling of carbon. Not surprisingly, several known carbon cyclers/PHC degraders were differentially abundant between treatments in the intact soil cores. Genera like *Geobacter* have been found to degrade hydrocarbons anaerobically[75,85] (in addition to oxidizing iron),[86] and some *Pseudomonas*, *Polaromonas*, *Cellulomonas*, and *Rhodoferax* species are known aerobic degraders.[87−91] Supporting the occurrence of anaerobic hydrocarbon degradation was the presence of a number of known syntrophic bacteria. For instance, some members of the *Syntrophus* and *Smithella* genera are secondary fermentative bacteria that oxidize intermediate products like propionate and benzoate and release H_2 and acetate.[75] Some *Corynebacterium* species secrete phosphatases that hydrolyze extracellular organophosphates, liberating phosphate that may then be taken up by bacterial P transport systems.[92] *Thauera* is a hydrogenotrophic denitrifier and produces benzylsuccinate synthase, which helps to catalyze anaerobic toluene degradation.[77,93] Syntrophic associations typically involve H_2- or acetate-consuming methanogenic archaea that perform the last step of the anaerobic carbon cycle by releasing methane.[75] Methanogenic archaea may use CO_2 (from hydrocarbon degradation) or H_2 (from propionate and benzoate degradation) to generate CH_4, which may then be used by *Methylobacterium* to generate formate as an intermediate.[86] Electrons generated during the oxidation of formate to CO_2 can be transferred to nitrate reductase of *Methylobacterium* or other denitrifiers.[94] Overall, these results suggest that the dominant processes underlying hydrocarbon degradation in the soils studied here are aerobic and ostensibly largely dictated by *Pseudomonas* and *Polaromonas*. However, anaerobic cometabolism and syntrophy[95] should not be overlooked as important agents of bioremediation in northern soils.

Bioremediation of PHC-contaminated sites is challenging due to mineral precipitation and bacterial overgrowth from eutrophic biostimulatory solutions. The mechanisms by which targeted biostimulatory solutions enhance bioremediation or foul distribution systems are unclear, particularly due to unrepresentative overprocessed soil samples used in laboratory studies of PHC degradation. Here, we confirmed our hypotheses that (i) optimized phosphate bioavailability would outperform generic biostimulatory solutions in promoting hydrocarbon degradation and (ii) oligotrophic biostimulation was more effective than eutrophic approaches. Fine-scale studies such as our study that optimize phosphate bioavailability and use intact soil cores have a key role in generating novel solutions for in situ bioremediation of PHCs.

■ ASSOCIATED CONTENT

Supporting Information

The Supporting Information is available free of charge at https://pubs.acs.org/doi/10.1021/acs.est.1c01113.

Supporting methods (biostimulatory solution decision tree rationale), supporting figures, and supporting tables (PDF)

■ AUTHOR INFORMATION

Corresponding Authors

Steven D. Mamet − *College of Agriculture and Bioresources, Department of Soil Science, University of Saskatchewan, Saskatoon, Saskatchewan S7N 5A8, Canada;* orcid.org/0000-0002-3510-3814; Email: steven.mamet@usask.ca

Steven D. Siciliano − *College of Agriculture and Bioresources, Department of Soil Science, University of Saskatchewan, Saskatoon, Saskatchewan S7N 5A8, Canada;* orcid.org/0000-0002-8994-3341; Email: steven.siciliano@usask.ca

Authors

Amy Jimmo − *College of Agriculture and Bioresources, Department of Soil Science, University of Saskatchewan, Saskatoon, Saskatchewan S7N 5A8, Canada*

Alexandra Conway − *College of Agriculture and Bioresources, Department of Soil Science, University of Saskatchewan, Saskatoon, Saskatchewan S7N 5A8, Canada*

Aram Teymurazyan − *Department of Physics, University of Regina, Regina, Saskatchewan S4S 0A2, Canada*

Alizera Talebitaher − *Department of Physics, University of Regina, Regina, Saskatchewan S4S 0A2, Canada*

Zisis Papandreou − *Department of Physics, University of Regina, Regina, Saskatchewan S4S 0A2, Canada*

Yu-Fen Chang − *Department of Physics, University of Regina, Regina, Saskatchewan S4S 0A2, Canada; Department of Mechanical and Marine Engineering, Western Norway University of Applied Sciences, Bergen, Norway; Nuclear Medicine and Radiation Biology Research Group, Department of Clinical Medicine, UiT The Arctic University of Norway, 9037 Tromsø, Norway*

Whitney Shannon − *Department of Chemistry, University of Saskatchewan, Saskatoon, Saskatchewan S7N 5C9, Canada; College of Agriculture and Bioresources, Department of Soil Science, University of Saskatchewan, Saskatoon, Saskatchewan S7N 5A8, Canada*

Derek Peak − *College of Agriculture and Bioresources, Department of Soil Science, University of Saskatchewan, Saskatoon, Saskatchewan S7N 5A8, Canada;* orcid.org/0000-0002-8876-3605

Complete contact information is available at: https://pubs.acs.org/10.1021/acs.est.1c01113

Author Contributions

The manuscript was written through contributions of all authors. All authors have given approval to the final version of the manuscript.

Funding

Funding came from the Natural Sciences and Engineering Research Council (NSERC) Industrial Research Chair grant (IRCSA 478012-13) sponsored by Federated Cooperatives Limited (FCL), the NSERC Engage and Supplement grant sponsored by CH2M Hill to S.D.S., the NSERC Subatomic Physics Discovery Grant to Z.P., and in-kind support from the Sylvia Fedoruk Canadian Centre for Nuclear Innovation at the University of Saskatchewan.

Notes

The authors declare no competing financial interest.

■ ACKNOWLEDGMENTS

The authors thank Alix Schebel, Lisa Moehlman, and the staff of the Saskatchewan Centre for Cyclotron Sciences (SCCS) for lab assistance. We are grateful for the help by Tom Palaia in completing this work. The authors declare no competing financial interest. The funders had no role in study design, data collection, and interpretation, or the decision to submit the work for publication.

■ REFERENCES

(1) Landrigan, P. J.; Fuller, R.; Acosta, N. J. R.; Adeyi, O.; Arnold, R.; Basu, N.; Baldé, A. B.; Bertollini, R.; Bose-O'Reilly, S.; Boufford, J. I.; Breysse, P. N.; Chiles, T.; Mahidol, C.; Coll-Seck, A. M.; Cropper, M. L.; Fobil, J.; Fuster, V.; Greenstone, M.; Haines, A.; Hanrahan, D.; Hunter, D.; Khare, M.; Krupnick, A.; Lanphear, B.; Lohani, B.; Martin, K.; Mathiasen, K. V.; McTeer, M. A.; Murray, C. J. L.; Ndahimananjara, J. D.; Perera, F.; Potočnik, J.; Preker, A. S.; Ramesh, J.; Rockström, J.; Salinas, C.; Samson, L. D.; Sandilya, K.; Sly, P. D.; Smith, K. R.; Steiner, A.; Stewart, R. B.; Suk, W. A.; van Schayck, O. C. P.; Yadama, G. N.; Yumkella, K.; Zhong, M. The Lancet Commission on pollution and health. *Lancet* **2018**, *391*, 462−512.

(2) Carré, F.; Caudeville, J.; Bonnard, R.; Bert, V.; Boucard, P.; Ramel, M. Soil Contamination and Human Health: A Major Challenge for Global Soil Security. *Glob. Soil Secur.* **2017**, 275−295.

(3) Panagos, P.; Van Liedekerke, M.; Yigini, Y.; Montanarella, L. Contaminated sites in Europe: review of the current situation based on data collected through a European network. *J. Environ. Public Health* **2013**, *2013*, 1−11.

(4) Horta, A.; Malone, B.; Stockmann, U.; Minasny, B.; Bishop, T. F. A.; McBratney, A. B.; Pallasser, R.; Pozza, L. Potential of integrated field spectroscopy and spatial analysis for enhanced assessment of soil contamination: A prospective review. *Geoderma* **2015**, *241-242*, 180−209.

(5) Amponsah, N. Y.; Wang, J.; Zhao, L. A review of life cycle greenhouse gas (GHG) emissions of commonly used ex-situ soil treatment technologies. *J. Cleaner Prod.* **2018**, *186*, 514−525.

(6) Atlas, R. M. Microbial degradation of petroleum hydrocarbons: an environmental perspective. *Microbiol. Rev.* **1981**, *45*, 180−209.

(7) Atlas, R. M.; Bartha, R. Degradation and mineralization of petroleum in sea water: limitation by nitrogen and phosphorous. *Biotechnol. Bioeng.* **1972**, *14*, 309−318.

(8) Miri, S.; Naghdi, M.; Rouissi, T.; Kaur Brar, S.; Martel, R. Recent biotechnological advances in petroleum hydrocarbons degradation under cold climate conditions: A review. *Crit. Rev. Environ. Sci. Technol.* **2019**, *49*, 553−586.

(9) Snape, I.; Riddle, M. J.; Filler, D. M.; Williams, P. J. Contaminants in freezing ground and associated ecosystems: key issues at the beginning of the new millennium. *Polar Record* **2003**, *39*, 291−300.

(10) Braddock, J. F.; Ruth, M. L.; Catterall, P. H.; Walworth, J. L.; McCarthy, K. A. Enhancement and Inhibition of Microbial Activity in Hydrocarbon-Contaminated Arctic Soils: Implications for Nutrient-Amended Bioremediation. *Environ. Sci. Technol.* **1997**, *31*, 2078−2084.

(11) Johnson, P.; Lundegard, P.; Liu, Z. Source Zone Natural Attenuation at Petroleum Hydrocarbon Spill Sites—I: Site-Specific Assessment Approach. *Ground Water Monit. Remediat.* **2006**, *26*, 82−92.

(12) Siciliano, S. D.; Chen, T.; Phillips, C.; Hamilton, J.; Hilger, D.; Chartrand, B.; Grosskleg, J.; Bradshaw, K.; Carlson, T.; Peak, D. Total phosphate influences the rate of hydrocarbon degradation but phosphate mineralogy shapes microbial community composition in cold-region calcareous soils. *Environ. Sci. Technol.* **2016**, *50*, 5197−5206.

(13) Bulmer, D.; Hamilton, J.; Kar, G.; Dhillon, G.; Si, B. C.; Peak, D. Effects of Citrate on the Rates and Mechanisms of Phosphate Adsorption and Desorption on a Calcareous Soil. *Soil Sci. Soc. Am. J.* **2019**, *83*, 332−338.

(14) Bulmer, D.; Kar, G.; Hamilton, J.; Siciliano, S.; Peak, D. Extent and Mechanism of Interaction between Phosphate and Citrate in a Calcareous Soil. *Soil Sci. Soc. Am. J.* **2018**, *82*, 315−322.

(15) Chen, T.; Philips, C.; Hamilton, J.; Chartbrand, B.; Grosskleg, J.; Bradshaw, K.; Carlson, T.; Timlick, K.; Peak, D.; Siciliano, S. D. Citrate addition increased phosphorus bioavailability and enhanced gasoline bioremediation. *J. Environ. Qual.* **2017**, *46*, 975−983.

(16) Roy, A.; Dutta, A.; Pal, S.; Gupta, A.; Sarkar, J.; Chatterjee, A.; Saha, A.; Sarkar, P.; Sar, P.; Kazy, S. K. Biostimulation and bioaugmentation of native microbial community accelerated bioremediation of oil refinery sludge. *Bioresour. Technol.* **2018**, *253*, 22−32.

(17) Meckenstock, R. U.; Boll, M.; Mouttaki, H.; Koelschbach, J. S.; Cunha Tarouco, P.; Weyrauch, P.; Dong, X.; Himmelberg, A. M. Anaerobic degradation of benzene and polycyclic aromatic hydrocarbons. *J. Mol. Microbiol. Biotechnol.* **2016**, *26*, 92−118.

(18) Molina-Barahona, L.; Rodríguez-Vázquez, R.; Hernández-Velasco, M.; Vega-Jarquín, C.; Zapata-Pérez, O.; Mendoza-Cantú, A.; Albores, A. Diesel removal from contaminated soils by biostimulation and supplementation with crop residues. *Appl. Soil Ecol.* **2004**, *27*, 165−175.

(19) Mamet, S. D.; Ma, B.; Ulrich, A.; Schryer, A.; Siciliano, S. D. Who is the rock miner and who is the hunter? The use of heavy-oxygen labeled phosphate ($P^{18}O_4$) to differentiate between C and P fluxes in a benzene-degrading consortium. *Environ. Sci. Technol.* **2018**, *52*, 1773−1786.

(20) Dong, X.; Greening, C.; Brüls, T.; Conrad, R.; Guo, K.; Blaskowski, S.; Kaschani, F.; Kaiser, M.; Laban, N. A.; Meckenstock, R. U. Fermentative Spirochaetes mediate necromass recycling in anoxic hydrocarbon-contaminated habitats. *ISME J.* **2018**, *12*, 2039−2050.

(21) Shahi, A.; Aydin, S.; Ince, B.; Ince, O. Evaluation of microbial population and functional genes during the. bioremediation of petroleum-contaminated soil as an effective monitoring approach. *Ecotoxicol. Environ. Saf.* **2016**, *125*, 153−160.

(22) Gao, Y. C.; Guo, S. H.; Wang, J. N.; Li, D.; Wang, H.; Zeng, D. H. Effects of different remediation treatments on crude oil contaminated saline soil. *Chemosphere* **2014**, *117*, 486−493.

(23) Chaîneau, C. H.; Rougeux, G.; Yéprémian, C.; Oudot, J. Effects of nutrient concentration on the biodegradation of crude oil and associated microbial populations in the soil. *Soil Biol. Biochem.* **2005**, *37*, 1490−1497.

(24) Balba, M. T.; Al-Awadhi, N.; Al-Daher, R. Bioremediation of oil-contaminated soil: microbiological methods for feasibility assessment and field evaluation. *J. Microbiol. Methods* **1998**, *32*, 155−164.

(25) Lewis, J.; Sjöstrom, J. Optimizing the experimental design of soil columns in saturated and unsaturated transport experiments. *J. Contam. Hydrol.* **2010**, *115*, 1−13.

(26) Hyde, K.; Ma, W.; Obal, T.; Bradshaw, K.; Carlson, T.; Mamet, S.; Siciliano, S. D. Incremental sampling methodology for petroleum hydrocarbon contaminated soils: volume estimates and remediation strategies. *Soil Sediment Contam.* **2019**, *28*, 51−64.

(27) Brewer, R.; Peard, J.; Heskett, M. A Critical Review of Discrete Soil Sample Data Reliability: Part 1-Field Study Results. *Soil Sediment Contam.* **2017**, *26*, 1−22.

(28) Brewer, R.; Peard, J.; Heskett, M. A Critical Review of Discrete Soil Sample Data Reliability: Part 2-Implications. *Soil Sediment Contam.* **2017**, *26*, 23−44.

(29) Chang, Y.-F.; Siciliano, S. D.; Mamet, S.; Conway, A. J.; Schebel, A.; Shannon, W.; Christopher, K.; Thompson, K.; Talebitaher, A.; Papandreou, Z.; Teymurazyan, A. Applying a Modular PET System to Investigate Bioremediation of Subsurface Contamination: A Proof-of-Principle Study. *J. Phys.: Conf. Ser.* **2018**, *1120*, No. 012077.

(30) Schmidt, M. P.; Mamet, S. D.; Ferrieri, R. A.; Peak, D.; Siciliano, S. D. From the Outside in: An Overview of Positron Imaging of Plant and Soil Processes. *Mol. Imaging* **2020**, *19*, No. 1536012120966405.

https://doi.org/10.1021/acs.est.1c01113
Environ. Sci. Technol. 2021, 55, 9864−9875

(31) Kinsella, K.; Schlyer, D. J.; Fowler, J. S.; Martinez, R. J.; Sobecky, P. A. Evaluation of positron emission tomography as a method to visualize subsurface microbial processes. *J. Hazard. Mater.* **2012**, *213-214*, 498−501.
(32) Thorpe, C. L.; Williams, H. A.; Boothman, C.; Lloyd, J. R.; Morris, K. Positron emission tomography to visualise in-situ microbial metabolism in natural sediments. *Appl. Radiat. Isot.* **2019**, *144*, 104−110.
(33) CH2M HILL Canada Limited *Semiannual Routine Monitoring and Supplemental Phase II ESA Report: Old Crow Nursing Station. Final Draft. Prepared for the Government of Yukon, Site Assessment and Remediation Unit*; July 2018, 2018.
(34) Lee, S.; Kross, B.; McKisson, J.; McKisson, J. E.; Weisenberger, A. G.; Xi, W.; Zorn, C.; Howell, C. R.; Reid, C. D.; Smith, M. P. PhytoPET: Design and Initial Results of Modular PET for Plant Biology In *2012 IEEE Nuclear Science Symposium and Medical Imaging Conference Record (NSS/MIC)*; Yu, B., Ed. Anaheim, CA, USA, 2012; pp. 1323−1325.
(35) Weisenberger, A. G.; Dong, H.; Kross, B.; Lee, S. J.; McKisson, J.; McKisson, J. E.; Xi, W.; Zorn, C.; Howell, C. R.; Crowell, A. S.; Cumberbatch, L.; Reid, C. D.; Smith, M. F.; Stolin, A. Development of PhytoPET: a Plant Imaging PET System. In *2011 IEEE Nuclear Science Symposium Conference Record*; Chmeissani, M., Ed. IEEE: Valencia, Spain, 2011; pp. 275−278.
(36) Weisenberger, A. G.; Kross, B.; Lee, S. J.; McKisson, J.; McKisson, J. E.; Xi, W.; Zorn, C.; Howell, C. R.; Crowell, A. S.; Reid, C. D.; Smith, M. Nuclear physics detector technology applied to plant biology research. *Nucl. Inst. Methods Phys. Res. A* **2013**, *718*, 157−159.
(37) Talebitaher, A.; Chang, Y.; Thompson, K.; Papandreou, Z.; Mamet, S.; Siciliano, S.; Lee, S.; McKisson, J.; Kross, B.; Teymurazyan, A. In *BioPET: Dedicated plant and soil microorganism positron emission tomography system*, Proceedings of 38th Annual Conference of the Canadian Nuclear Society, Saskatoon, SK, 3−6 June 2018, 2018; Saskatoon, SK, 2018.
(38) NEMA *Performance Measurements of Small Animal Positron Emission Tomographs*; Rosslyn, Virginia, USA, 2008.
(39) Shepp, L. A.; Vardi, Y. Maximum likelihood reconstruction for emission tomography. *IEEE Trans. Med. Imaging* **1982**, *1*, 113−122.
(40) Merlin, T.; Stute, S.; Benoit, D.; Bert, J.; Carlier, T.; Comtat, C.; Filipovic, M.; Lamare, F.; Visvikis, D. CASToR: a generic data organization and processing code framework for multi-modal and multi-dimensional tomographic reconstruction. *Phys. Med. Biol.* **2018**, *63*, 185005.
(41) Schindelin, J.; Arganda-Carreras, I.; Frise, E.; Kaynig, V.; Longair, M.; Pietzsch, T.; Preibisch, S.; Rueden, C.; Saalfeld, S.; Schmid, B.; Tinevez, J. Y.; White, D. J.; Hartenstein, V.; Eliceiri, K.; Tomancak, P.; Cardona, A. Fiji: an open-source platform for biological-image analysis. *Nat. Methods* **2012**, *9*, 676−682.
(42) Abràmoff, M. D.; Magalhães, P. J.; Ram, S. J. Image processing with ImageJ. *Biophoton. Int.* **2004**, *11*, 36−42.
(43) Bolte, S.; Cordelières, F. P. A guided tour into subcellular colocalization analysis in light microscopy. *J. Microsc.* **2006**, *224*, 213−232.
(44) Ordonez, A. A.; Weinstein, E. A.; Bambarger, L. E.; Saini, V.; Chang, Y. S.; DeMarco, V. P.; Klunk, M. H.; Urbanowski, M. E.; Moulton, K. L.; Murawski, A. M.; Pokkali, S.; Kalinda, A. S.; Jain, S. K. A systematic approach for developing bacteria-specific imaging tracers. *J. Nucl. Med.* **2017**, *58*, 144−150.
(45) CCME. *Canada-wide Standards for Petroleum Hydrocarbons (PHC) in Soil*. CCME Council of Ministers: Winnipeg, MB, 2008; p 8.
(46) Smets, W.; Leff, J. W.; Bradford, M. A.; McCulley, R. L.; Lebeer, S.; Fierer, N. A method for simultaneous measurement of soil bacterial abundances and community composition via 16S rRNA gene sequencing. *Soil Biol. Biochem.* **2016**, *96*, 145−151.
(47) Tringe, S. G.; Hugenholtz, P. A renaissance for the pioneering 16S rRNA gene. *Curr. Opin. Microbiol.* **2008**, *11*, 442−446.
(48) Woese, C. R. Bacterial evolution. *Microbiol. Rev.* **1987**, *51*, 221−271.
(49) Fierer, N.; Jackson, J. A.; Vilgalys, R.; Jackson, R. B. Assessment of soil microbial community structure by use of taxon-specific quantitative PCR assays. *Appl. Environ. Microbiol.* **2005**, *71*, 4117−4120.
(50) Martin, M. Cutadapt removes adapter sequences from high-throughput sequencing reads. *EMBnet* **2011**, *17*, 3.
(51) Bolyen, E.; Rideout, J. R.; Dillon, M. R.; Bokulich, N. A.; Abnet, C. C.; al-Ghalith, G. A.; Alexander, H.; Alm, E. J.; Arumugam, M.; Asnicar, F.; Bai, Y.; Bisanz, J. E.; Bittinger, K.; Brejnrod, A.; Brislawn, C. J.; Brown, C. T.; Callahan, B. J.; Caraballo-Rodríguez, A. M.; Chase, J.; Cope, E. K.; da Silva, R.; Diener, C.; Dorrestein, P. C.; Douglas, G. M.; Durall, D. M.; Duvallet, C.; Edwardson, C. F.; Ernst, M.; Estaki, M.; Fouquier, J.; Gauglitz, J. M.; Gibbons, S. M.; Gibson, D. L.; Gonzalez, A.; Gorlick, K.; Guo, J.; Hillmann, B.; Holmes, S.; Holste, H.; Huttenhower, C.; Huttley, G. A.; Janssen, S.; Jarmusch, A. K.; Jiang, L.; Kaehler, B. D.; Kang, K. B.; Keefe, C. R.; Keim, P.; Kelley, S. T.; Knights, D.; Koester, I.; Kosciolek, T.; Kreps, J.; Langille, M. G. I.; Lee, J.; Ley, R.; Liu, Y.-X.; Loftfield, E.; Lozupone, C.; Maher, M.; Marotz, C.; Martin, B. D.; McDonald, D.; McIver, L. J.; Melnik, A. V.; Metcalf, J. L.; Morgan, S. C.; Morton, J. T.; Naimey, A. T.; Navas-Molina, J. A.; Nothias, L. F.; Orchanian, S. B.; Pearson, T.; Peoples, S. L.; Petras, D.; Preuss, M. L.; Pruesse, E.; Rasmussen, L. B.; Rivers, A.; Robeson, M. S.; Rosenthal, P.; Segata, N.; Shaffer, M.; Shiffer, A.; Sinha, R.; Song, S. J.; Spear, J. R.; Swafford, A. D.; Thompson, L. R.; Torres, P. J.; Trinh, P.; Tripathi, A.; Turnbaugh, P. J.; Ul-Hasan, S.; van der Hooft, J. J. J.; Vargas, F.; Vázquez-Baeza, Y.; Vogtmann, E.; von Hippel, M.; Walters, W.; Wan, Y.; Wang, M.; Warren, J.; Weber, K. C.; Williamson, C. H. D.; Willis, A. D.; Xu, Z. Z.; Zaneveld, J. R.; Zhang, Y.; Zhu, Q.; Knight, R.; Caporaso, J. G. Reproducible, interactive, scalable and extensible microbiome data science using QIIME 2. *Nat. Biotechnol.* **2019**, *37*, 852−857.
(52) Rognes, T.; Flouri, T.; Nichols, B.; Quince, C.; Mahé, F. VSEARCH: a versatile open source tool for metagenomics. *PeerJ* **2016**, *4*, No. e2584.
(53) Bokulich, N. A.; Subramanian, S.; Faith, J. J.; Gevers, D.; Gordon, J. I.; Knight, R.; Mills, D. A.; Caporaso, J. G. Quality-filtering vastly improves diversity estimates from Illumina amplicon sequencing. *Nat. Methods* **2013**, *10*, 57−59.
(54) Amir, A.; McDonald, D.; Navas-Molina, J. A.; Kopylova, E.; Morton, J. T.; Zech Xu, Z.; Kightley, E. P.; Thompson, L. R.; Hyde, E. R.; Gonzalez, A.; Knight, R. Deblur Rapidly Resolves Single-Nucleotide Community Sequence Patterns. *mSystems* **2017**, *2*, No. e00191-16.
(55) Yilmaz, P.; Parfrey, L. W.; Yarza, P.; Gerken, J.; Pruesse, E.; Quast, C.; Schweer, T.; Peplies, J.; Ludwig, W.; Glöckner, F. O. The SILVA and "All-species Living Tree Project (LTP)" taxonomic frameworks. *Nucleic Acids Res.* **2014**, *42*, D643−D648.
(56) McDonald, D.; Clemente, J. C.; Kuczynski, J.; Rideout, J. R.; Stombaugh, J.; Wendel, D.; Wilke, A.; Huse, S.; Hufnagle, J.; Meyer, F.; Knight, R.; Caporaso, J. G. The Biological Observation Matrix (BIOM) format or: how I learned to stop worrying and love the ome-ome. *GigaScience* **2012**, *1*, 7−7.
(57) R Core Team *R: A language and environment for statistical computing*. R Foundation for Statistical Computing, Vienna, Austria. https://www.R-project.org/, 2020.
(58) McMurdie, P. J.; Holmes, S. phyloseq: An R package for reproducible interactive analysis and graphics of microbiome census data. *PLoS One* **2013**, *8*, No. e61217.
(59) McDonald, D.; Price, M. N.; Goodrich, J.; Nawrocki, E. P.; DeSantis, T. Z.; Probst, A.; Andersen, G. L.; Knight, R.; Hugenholtz, P. An improved Greengenes taxonomy with explicit ranks for ecological and evolutionary analyses of bacteria and archaea. *ISME J.* **2012**, *6*, 610−618.
(60) Janssen, S.; McDonald, D.; Gonzalez, A.; Navas-Molina, J. A.; Jiang, L.; Xu, Z. Z.; Winker, K.; Kado, D. M.; Orwoll, E.; Manary, M.; Mirarab, S.; Knight, R. Phylogenetic placement of exact amplicon sequences improves associations with clinical information. *mSystems* **2018**, *3*, No. e00021-18.

https://doi.org/10.1021/acs.est.1c01113
Environ. Sci. Technol. 2021, 55, 9864−9875

(61) Mirarab, S.; Nguyen, N.; Warnow, T. SEPP: SATé-Enabled Phylogenetic Placement. In *Proceedings of the Pacific Symposium on Biocomputing 2012*; Altman, R. B.; Dunker, A. K.; Hunter, L.; Murray, T.; Klein, T. E., Eds. World Scientific Publishing Co: Hackensack, NJ, 2012; pp. 247−258.
(62) Felsenstein, J.; Archie, J.; Day, W.; Maddison, W.; Meacham, C.; Rohlf, F.; Swofford, D., The Newick tree format. In 1986. http://evolution.genetics.washington.edu/phylip/newicktree.html, 2000.
(63) Paradis, E.; Schliep, K. ape 5.0: an environment for modern phylogenetics and evolutionary analyses in R. *Bioinformatics* **2019**, *35*, 526−528.
(64) Keck, F.; Rimet, F.; Bouchez, A.; Franc, A. phylosignal: an R package to measure, test, and explore the phylogenetic signal. *Ecol. Evol.* **2016**, *6*, 2774−2780.
(65) Bolker, B.; Butler, M.; Cowan, P.; Vienne, D. d.; Eddelbuettel, D.; Holder, M.; Jombart, T.; Kembel, S.; Michonneau, F.; Orme, D.; O'Meara, B.; Paradis, E.; Regetz, J.; Zwickl, D. *Phylobase: Base Package for Phylogenetic Structures and Comparative Data. R package version 0.8.10*. https://CRAN.R-project.org/package=phylobase, 2020.
(66) Pinheiro, J.; Bates, D.; DebRoy, S.; Sarkar, D.; R Core Team. nlme: Linear and Nonlinear Mixed Effects Models. R package version 3.1−148. https://CRAN.R-project.org/package=nlme, 2020.
(67) Zuur, A. F. *Mixed Effects Models and Extensions in Ecology with R*. Springer: New York, NY, 2009; p 579, DOI: 10.1007/978-0-387-87458-6.
(68) Oksanen, J.; Blanchet, F. G.; Friendly, M.; Kindt, R.; Legendre, P.; McGlinn, D.; Minchin, P. R.; O'Hara, R. B.; Simpson, G. L.; Solymos, P.; Stevens, M. H. H.; Szoecs, E.; Wagner, H. *vegan: Community Ecology Package. R Package version 2.5-7*. https://CRAN.R-project.org/package=vegan, 2020.
(69) Palarea-Albaladejo, J.; Martín-Fernández, J. A. zCompositions — R package for multivariate imputation of left-censored data under a compositional approach. *Chemom. Intell. Lab. Syst.* **2015**, *143*, 85−96.
(70) Gloor, G. B.; Macklaim, J. M.; Pawlowsky-Glahn, V.; Egozcue, J. J. Microbiome datasets are compositional: And this is not optional. *Front. Microbiol.* **2017**, *8*, 2224.
(71) Gloor, G. B.; Reid, G. Compositional analysis: a valid approach to analyze microbiome high-throughput sequencing data. *Can. J. Microbiol.* **2016**, *62*, 692−703.
(72) Vyang, I. V.; Chen, E.; Hasseman, J. P.; Liang, W.; Frank, B. C.; Wang, S.; Sharov, V.; Saeed, A. I.; White, J.; Li, J.; Lee, N. H.; Yeatman, T. J.; Quackenbush, J. Within the fold: assessing differential expression measures and reproducibility in microarray assays. *Genome Biol.* **2002**, *3*, No. research0062.1.
(73) Butler, J. E.; He, Q.; Nevin, K. P.; He, Z.; Zhou, J.; Lovley, D. R. Genomic and microarray analysis of aromatics degradation in *Geobacter metallireducens* and comparison to a *Geobacter* isolate from a contaminated field site. *BMC Genom.* **2007**, *8*, 180−180.
(74) Fowler, S. J. *Syntrophic hydrocarbon metabolism under methanogenic conditions*. Doctoral Thesis, University of Calgary: Calgary, AB, 2014.
(75) Yang, S.; Wen, X.; Shi, Y.; Liebner, S.; Jin, H.; Perfumo, A. Hydrocarbon degraders establish at the costs of microbial richness, abundance and keystone taxa after crude oil contamination in permafrost environments. *Sci. Rep.* **2016**, *6*, 37473.
(76) Correa-García, S.; Pande, P.; Séguin, A.; St-Arnaud, M.; Yergeau, E. Rhizoremediation of petroleum hydrocarbons: a model system for plant microbiome manipulation. *Microb. Biotechnol.* **2018**, *11*, 819−832.
(77) Mao, Y.; Xia, Y.; Zhang, T. Characterization of *Thauera*-dominated hydrogen-oxidizing autotrophic denitrifying microbial communities by using high-throughput sequencing. *Bioresour. Technol.* **2013**, *128*, 703−710.
(78) Sorger-Herrmann, U.; Taniguchi, H.; Wendisch, V. F. Regulation of the pstSCAB operon in *Corynebacterium glutamicum* by the regulator of acetate metabolism RamB. *BMC Microbiol.* **2015**, *15*, 113.
(79) Kim, J.; Lee, A. H.; Chang, W. Enhanced bioremediation of nutrient-amended, petroleum hydrocarbon-contaminated soils over a cold-climate winter: The rate and extent of hydrocarbon biodegradation and microbial response in a pilot-scale biopile subjected to natural seasonal freeze-thaw temperatures. *Sci. Total Environ.* **2018**, *612*, 903−913.
(80) Environment and Climate Change Canada Technical Documentation - Digital Archive of Canadian Climatological Data. https://climate.weather.gc.ca/doc/Technical_Documentation.pdf (1 October 2019),
(81) Franklin, R. B.; Mills, A. L. *The spatial distribution of microbes in the environment*. Springer: 2007, DOI: 10.1007/978-1-4020-6216-2.
(82) Ramette, A.; Tiedje, J. M. Multiscale responses of microbial life to spatial distance and environmental heterogeneity in a patchy ecosystem. *Proc. Natl. Acad. Sci.* **2007**, *104*, 2761−2766.
(83) Lacal, J., The Potential of Hydrocarbon Chemotaxis to Increase Bioavailability and Biodegradation Efficiency. In *Cellular Ecophysiology of Microbe*; Krell, T., Ed. Springer International Publishing: Cham, 2017; pp. 1−14, DOI: 10.1007/978-3-319-20796-4_3-1.
(84) Aufrecht, J. A.; Fowlkes, J. D.; Bible, A. N.; Morrell-Falvey, J.; Doktycz, M. J.; Retterer, S. T. Pore-scale hydrodynamics influence the spatial evolution of bacterial biofilms in a microfluidic porous network. *PLoS One* **2019**, *14*, No. e0218316.
(85) Kimes, N. E.; Callaghan, A. V.; Aktas, D. F.; Smith, W. L.; Sunner, J.; Golding, B. T.; Drozdowska, M.; Hazen, T. C.; Suflita, J. M.; Morris, P. J. Metagenomic analysis and metabolite profiling of deep−sea sediments from the Gulf of Mexico following the Deepwater Horizon oil spill. *Front. Microbiol.* **2013**, *4*, 1−17.
(86) Joshi, M. N.; Dhebar, S. V.; Dhebar, S. V.; Bhargava, P.; Pandit, A.; Patel, R. P.; Saxena, A.; Bagatharia, S. B. Metagenomics of petroleum muck: revealing microbial diversity and depicting microbial syntrophy. *Arch. Microbiol.* **2014**, *196*, 531−544.
(87) Aburto, A.; Peimbert, M. Degradation of a benzene−toluene mixture by hydrocarbon-adapted bacterial communities. *Ann. Microbiol.* **2011**, *61*, 553−562.
(88) Palleroni, N. J.; Pieper, D. H.; Moore, E. R. B. Microbiology of Hydrocarbon-Degrading *Pseudomonas*. In *Handbook of Hydrocarbon and Lipid Microbiology*; Timmis, K. N., Ed. Springer Berlin Heidelberg: Berlin, Heidelberg, 2010, pp. 1787−1798, DOI: 10.1007/978-3-540-77587-4_129.
(89) Parales, R. E. Hydrocarbon Degradation by Betaproteobacteria. In *Handbook of Hydrocarbon and Lipid Microbiology*; Timmis, K. N., Ed. Springer Berlin Heidelberg: Berlin, Heidelberg, 2010, pp. 1715−1724, DOI: 10.1007/978-3-540-77587-4_121.
(90) Riis, V.; Kleinsteuber, S.; Babel, W. Influence of high salinities on the degradation of diesel fuel by bacterial consortia. *Can. J. Microbiol.* **2003**, *49*, 713−721.
(91) Whyte, L. G.; Bourbonniére, L.; Greer, C. W. Biodegradation of petroleum hydrocarbons by psychrotrophic *Pseudomonas* strains possessing both alkane (alk) and naphthalene (nah) catabolic pathways. *Appl. Environ. Microbiol.* **1997**, *63*, 3719−3723.
(92) Burkovski, A., *Corynebacteria: Genomics and Molecular Biology*. Caister Academic Press: Norfolk, UK, 2008; p 340.
(93) Leuthner, B.; Leutwein, C.; Schulz, H.; Hörth, P.; Haehnel, W.; Schiltz, E.; Schägger, H.; Heider, J. Biochemical and genetic characterization of benzylsuccinate synthase from *Thauera aromatica*: a new glycyl radical enzyme catalysing the first step in anaerobic toluene metabolism. *Mol. Microbiol.* **1998**, *28*, 615−628.
(94) Ingledew, W. J.; Poole, R. K. The respiratory chains of *Escherichia coli*. *Microbiol. Rev.* **1984**, *48*, 222.
(95) Pérez-de-Mora, A.; Zila, A.; McMaster, M. L.; Edwards, E. A. Bioremediation of Chlorinated Ethenes in Fractured Bedrock and Associated Changes in Dechlorinating and Nondechlorinating Microbial Populations. *Environ. Sci. Technol.* **2014**, *48*, 5770−5779.